


Intermediate-Temperature Proton Exchange Membranes Based on Cerium Ultraphosphate Compositized with Polybenzimidazole


To cite this article: Oksana Zholobko *et al* 2022 *J. Electrochem. Soc.* **169** 094505

View the [article online](#) for updates and enhancements.






 The Electrochemical Society
Advancing solid state & electrochemical science & technology

242nd ECS Meeting
Oct 9 – 13, 2022 • Atlanta, GA, US
Presenting more than 2,400
technical abstracts in 50 symposia

ECS Plenary Lecture
featuring
M. Stanley Whittingham,
Binghamton University
Nobel Laureate –
2019 Nobel Prize in Chemistry

 **Register now!**





Intermediate-Temperature Proton Exchange Membranes Based on Cerium Ultraphosphate Compositing with Polybenzimidazole

Oksana Zholobko,^{1,z} John Hurley,² Xiang-Fa Wu,^{1,z} Ted Aulich,^{2,z} and Jivan Thakare^{2,*}

¹Department of Mechanical Engineering, North Dakota State University, Fargo, North Dakota 58108, United States of America

²Energy and Environmental Research Center, University of North Dakota, Grand Forks, North Dakota 58202, United States of America

This paper reports the rational fabrication and structural, thermal, mechanical and electrochemical characterization of a new type of intermediate-temperature (IT) polymer-inorganic composite (PIC) proton exchange membranes (PEMs) that are made of cerium ultraphosphate (CeP₃O₁₄—CUP) as the solid-state proton conductor compositing with a high-temperature (HT) polybenzimidazole (PBI) as the polymeric binder. Flexible PBI-CUP PIC membranes with the thickness of ~135 μm and CUP mass fraction of up to 75% were prepared by solution-casting without additional acid-doping (e.g., phosphoric acid). The proton conductivity of the fabricated IT-PIC-PEMs was up to 5.80 × 10⁻² S cm⁻¹ as measured from a prototype IT PEM fuel cell (PEMFC) operated at 200 °C in the humidified hydrogen and air environment. This type of IT-PIC-PEMs also demonstrated sufficient mechanical strength and flexibility, excellent thermal stability (up to 350 °C), and very good durability of the proton conductivity (within the test duration of 500 h). The present experimental study shows the promising future of the IT-PIC-PEMs for applications in various IT electrochemical processes including IT-PEMFCs, IT-electrolyzers, etc.

© 2022 The Electrochemical Society ("ECS"). Published on behalf of ECS by IOP Publishing Limited. [DOI: 10.1149/1945-7111/ac90f0]

Manuscript submitted April 28, 2022; revised manuscript received July 6, 2022. Published September 20, 2022.

Supplementary material for this article is available [online](#)

Development of durable proton-conducting membranes carrying high proton conductivity is fundamentally important to modern electrochemical processes, e.g., proton exchange membrane fuel cells (PEMFCs),^{1,2} electrolytic ammonia production,³⁻⁶ hydrogen separation,^{7,8} and electrolysis,⁹ among others.¹⁰⁻¹² To date, significant technical progress has been made in PEMFCs with the operating temperatures lower than 100 °C for mobile electricity generation to power portable electronics and ground vehicles, in which perfluorosulfonic polymer membranes (e.g., Nafion[®] membranes) play the dominant role as the proton exchange membranes (PEMs) due to their high proton conductivity (e.g., ~0.06 S cm⁻¹ for Nafion[®] 112 at 100% relative humidity and room temperature), high power density (>1.0 W cm⁻²), and high current density (>1.0 A cm⁻²),^{13,14} Yet, due to the material limitations of Nafion[®] such as its low glass transition temperature ($T_g = 111$ °C) and dehydration at a temperature higher than 100 °C, the low operating temperatures of PEMFCs have obvious technical disadvantages in the view of fuel cell performances, such as the low tolerance of the catalyst (Pt-nanoparticles) to fuel impurities (e.g., either CO or SO₂ impurities in reformed hydrogen fuels), a complex management strategy for liquid water, etc.^{15,16} It is technically desired to develop fuel cells that can be operated in the temperature range of 100 °C – 400 °C, i.e., intermediate-temperature fuel cells (ITFCs), which relies on high-performance intermediate-temperature (IT) PEMs with high and durable proton conductivity, low electrical conductivity and hydrogen/oxygen permeability, as well as high thermal stability, mechanical properties and structural integrity. The operating temperature of ITFCs is between that of current low-temperature (LT) PEMFCs and solid oxide fuel cells (SOFCs). The latter are typically classified as high-temperature (HT) fuel cells with the operating temperature between 500 °C – 1,000 °C for use in large-scale stationary electricity generation and cargo ship power generation, which quest highly anticorrosive electrode materials and sealants.¹⁷⁻¹⁹ Compared to LT PEMFCs, ITFCs have several technical advantages: (1) Effective suppression of anode catalyst poisoning due to fuel impurities, (2) enhancement of the kinetics of both electrode reactions and reduction of the mass loading of noble metal catalysts (e.g., Pt nanoparticles), (3) substantial simplification

of the water and heat management system, and (4) improvement of the fuel efficiency.^{20,21} Compared to SOFCs, ITFCs do not need costly HT materials, anticorrosive and sealing design, and additional startup system, among others. In short, ITFCs carry the technical advantages of both LT PEMFCs and HT SOFCs while overcoming their major disadvantages. In the view of fuel cell design and fabrication, IT PEM is the core functional component of ITFCs, which can be equivalently utilized in other electrochemical processes for economically viable electrolytic ammonia production and electrolysis for hydrogen generation at ITs, e.g., at the operating temperature of 300 °C.

In the past two decades, significant efforts have been devoted to exploring various IT PEMs for ITFCs and other IT electrochemical processes. Among others, phosphoric acid (H₃PO₄) doped polybenzimidazole (PBI) membranes have been intensively investigated in the temperature range of 120 °C – 220 °C.²²⁻²⁴ At the high acid-doping levels of 4 to 6 (in term of the number of H₃PO₄ molecules per polymer repeat unit), the proton migration in H₃PO₄-doped PBI membranes is along mainly with the acid (H₂PO₄⁻ - H⁺ - H₂PO₄⁻) or the acid and water (H₂PO₄⁻ - H⁺...H₂O) chain depending upon the water content through the Grotthus mechanism (hopping),²⁵ and the corresponding proton conductivity was measured about 4–7 × 10⁻² S cm⁻¹ (Ref. 26). Recently, significant improvement in the acid-doping of PBI membranes has been made with the acid-doping levels of up to 10–12 for post doped membranes and 20–30 for sol-gel PBI membranes.²⁷ Acid-doped PBI membrane electrode assemblies (MEAs) have been commercialized under the brand name Celtec[®] by the BASF Fuel Cell (Germany). Yet, the durability of acid-doped PBI membranes as PEMs is still a technical challenge due to degradation of the PBI membranes attacked by H₂O₂ and its radicals (e.g., -OH, -OOH, etc.), flooding and leaching of doped acids, etc.^{16,22-24} Most PBI polymers currently utilized in IT-PEMs are amorphous such as the typical m-PBI, which are more vulnerable under attack of radicals especially in the HT acidic environment. Among others, crosslinking of PBIs has been demonstrated as one of the technical options to suppress the PBI degradation and enhance the durability of the resulting acid-doped PBI membranes.²⁸⁻³² Other materials under intensive investigation for use as IT solid-state proton conductors include acidic phosphates, such as zirconium phosphate [Zr(HPO₄)₂],³³ cesium hydrogen phosphate (Cs₂HPO₄),³⁴ and cesium dihydrogen phosphate (CsH₂PO₄)^{35,36} at the work temperatures of 150 °C – 250 °C with the proton conductivity of

*Electrochemical Society Member.

^zE-mail: oksana.zholobko@ndsu.edu; xiangfa.wu@ndsu.edu; taulich@undeerc.org

up to 0.15 S cm^{-1} , heteropolyacids, pyrophosphates, etc. at the higher work temperatures.^{20,21} It needs to be mentioned that acidic phosphates belong to a family of solid acids with the general chemical formula $\text{M}_x\text{H}_y(\text{AO}_4)_z$ ($\text{M} = \text{Cs}, \text{K}, \text{Na}, \text{Li}, \text{NH}_4, \text{Rb}$; $\text{A} = \text{S}, \text{Se}, \text{As}, \text{P}$).^{37,38} Some types of such solid acids exhibit ordered hydrogen bond structure at room temperature and become disordered at HTs. Solid acids can exhibit hyperproton transition due to the Grothuss mechanism when the temperature is higher than certain values.³⁴ For instance, the crystal structure of cesium hydrogen sulfate (CsHSO_4) exhibits monoclinic below 141°C , and it switches to tetragonal when the temperature is higher than 141°C . Correspondingly, the proton conductivity of CsHSO_4 has 2–3 orders to increase up to the magnitude of 10^{-3} – $10^{-2} \text{ S cm}^{-1}$ (Ref. 37). In addition, recent experimental studies have shown that broad pyrophosphates of tetravalent elements (MP_2O_7 with $\text{M} = \text{Sn}, \text{Zr}, \text{Ti}$, and Ce) doped with small amounts of some low valency cations (e. g., In^{3+} , Al^{3+} , Mg^{2+} , Sb^{3+} , Sc^{3+} , and Ga^{3+}) exhibited noticeable proton conductivity ($>10^{-2} \text{ S cm}^{-1}$) in the temperature range of 150°C – 400°C under unhumidified conditions though different research groups reported wide deviations in the measured values of proton conductivity even for the same pyrophosphate.^{20,39–41} MP_2O_7 carries a cubic crystal structure with MO_6 octahedra and P_2O_7 units at the corners and edges, respectively, and such closely packed P_2O_7 units provide multiple proton bonding sites and transport pathways. These solid acids and pyrophosphates are typically fragile and cannot be directly formed into durable thin films for fuel cell tests. As a matter of fact, intensive investigations are still undergoing to composite these solid acids and pyrophosphates with plastic polymers (e.g., PBI) to form polymer-inorganic composite (PIC) PEMs for use in ITFCs. For instance, PBI- $\text{Sb}_{0.2}\text{Sn}_{0.8}\text{P}_2\text{O}_7$ composite PEMs with the thickness of $\sim 40 \mu\text{m}$ were prepared by solution-casting the blend of PBI with a fine powder of $\text{Sb}_{0.2}\text{Sn}_{0.8}\text{P}_2\text{O}_7$ (20 wt%) and dimethylacetamide (DMAc).⁴² The resulting PIC PEMs could achieve the proton conductivity of up to 0.04 S cm^{-1} at 240°C and the effective areal power density of 0.67 W cm^{-2} at 175°C when assembled into the IT-MEAs for a H_2/O_2 fuel cell. In addition, recent studies also considered using HT polymers such as polytetrafluoroethylene (PTFE) as the catalyst binder of the gas diffusion electrodes (GDEs) to improve the overall electrochemical performance of IT-PEMFCs based on H_3PO_4 -doped PBI membranes since the hydrophobicity of PTFE suppresses H_3PO_4 flooding and leaching as well as PTFE does not react with H_3PO_4 and can enhance the higher kinetic overpotential, among others.^{43–45}

Furthermore, researchers have also explored ultraphosphates, phytates, etc. for the potential use as IT PEMs for ITFCs.^{46–54} Ultraphosphate glass electrolytes, e.g., $\text{BaO-ZnO-P}_2\text{O}_5$, $30\text{Cs}_2\text{O-70P}_2\text{O}_5$, $30\text{ZnO-70P}_2\text{O}_5$, and $10\text{Cs}_2\text{O-20ZnO-70P}_2\text{O}_5$, were synthesized by means of the melt-quenching technique and they do not behave phase transition in a wide temperature range of 25°C – 250°C .^{46,47} The proton conductivity of such glass electrolyte disks with the thickness of 0.8 – 1.8 mm was measured as 1.0 – $1.7 \times 10^{-3} \text{ S cm}^{-1}$ in the temperature range of 200°C – 250°C on a hydrogen fuel cell, and the effective power density was 0.4 – 1.2 mW cm^{-2} . Yet, the release of H_3PO_4 due to the degradation of these glass electrolytes in fuel cell tests deteriorated their chemical

stability and therefore the performance durability of the fuel cells, which is possibly resulted from the not well-formed covalent ultraphosphate structures.

More recently in the research of solid-state proton conductors, cerium ultraphosphate ($\text{CeP}_5\text{O}_{14}$ -CUP) with the orthorhombic crystal structure was synthesized and tested as IT PEMs with the high proton conductivity. Several CUP synthesis routes have been explored and reported in the literature.^{48–54} When measured at the humidity of $\text{P}_{\text{H}_2\text{O}} = 0.15 \text{ atm}$, CUP exhibited high and stable proton conductivity of 0.02 S cm^{-1} at 120°C to 0.025 S cm^{-1} at 210°C , and the proton conductivity can maintain at 0.03 – 0.33 S cm^{-1} (Ref. 50). The IT proton-conducting mechanisms in CUP can be related to the Grothuss proton hopping mechanism at low humidity though additional experimental and theoretical investigations are still needed. Besides, thermogravimetric analysis (TGA) indicated that CUP carries the excellent structural stability up to 650°C . Thus, CUP is expected to be an excellent solid-state proton conductor for use as IT PEMs in ITFCs and other IT electrochemical processes. Yet, as-synthesized CUP powder consists of fragile particles in micrometer scales, which cannot be directly formed into thin membranes with sufficient structural integrity and mechanical durability. Therefore, in this study, we report a new type of IT-PIC-PEMs made of CUP powder as the solid-state proton conductor composited with HT m-PBI as the polymeric binder. The flexible PIC PEMs with the thickness of $\sim 135 \mu\text{m}$ and CUP mass fraction of up to 75% were fabricated by means of the low-cost solution-casting technique. Detailed crystal structure, microstructural morphology, thermal stability, mechanical properties, and proton conductivity of this type of IT-PIC-PEMs were characterized to show their technical feasibility for use in IT-PEMFCs. A conceptual single-stack IT-PEMFC installed with the present PIC PEM was prototyped and operated at 200°C with humidified hydrogen and air as the fuel and oxidant, respectively. The characteristic polarization curve (V - I diagram) and power density curve (P - I diagram) of this IT-PEMFC were obtained. The related performance mechanisms were explored and discussed. Consequently, conclusions and prospects of the present experimental study were summarized.

Experimental

Materials.—PBI S26 solution (with 26.2 wt% PBI polymer of $\text{M}_w \approx 35,000$, dissolved in 72.3 wt% DMAc in the presence of a 1.5 wt% LiCl stabilizer) and PBI films with the thickness of $55 \mu\text{m}$ were purchased from the PBI Performance Products Inc. (Charlotte, NC). The PBI S26 solution was further diluted with DMAc for the purpose of the present study of PEM fabrication. This specific PBI provided by the PBI Performance Products Inc. is coined with the trademark Celazole®, i.e., poly 2,2'-m-(phenylene)-5,5'-bibenzimidazole with the chemical structure as shown in Fig. 1, and is classified as m-PBI since the phenylene ring is meta-coordinated. In the bulk state this type of PBI carries the high thermal stability with its glass transition temperature T_g in the range of 425°C – 436°C , excellent chemical resistance, and sound retention of mechanical properties (e.g., the tensile strength of 160 MPa, Young's modulus of 5.9 GPa, and tensile strain at break of 3%) in a wide range of temperature due to its unique aromatic nuclei.^{55,56} In addition, cerium oxide (CeO_2) powder, phosphoric acid (H_3PO_4) (86 wt%),

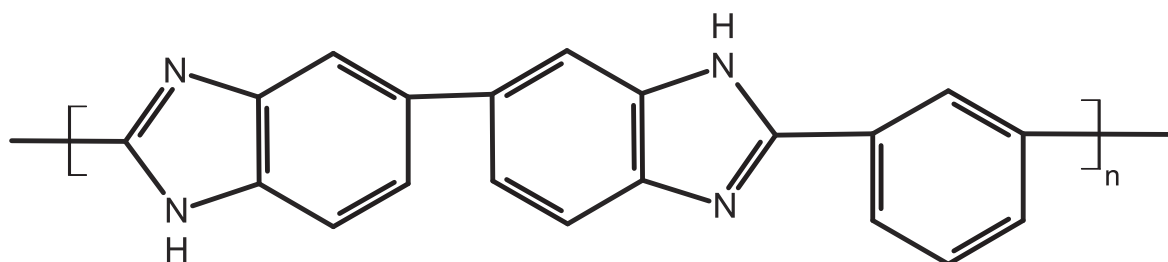


Figure 1. The chemical structure of m-PBI (Celazole®).

and DMAc anhydrous (99.8%) were purchased from the MilliporeSigma (St. Louis, MO). Pt catalyst nanoparticles (60 wt% platinum on Vulcan XC 72) and the gas diffusion layers (GDLs) (CT carbon cloths with microporous layers) were purchased from the Fuel Cell Store (College Station, TX).

Synthesis of solid-state proton conductor-CUP.—Cerium ultra-phosphate ($\text{CeP}_5\text{O}_{14}$ —CUP) was synthesized from CeO_2 and H_3PO_4 (the molar ratio of Ce/P = 1: 12) by a HT solution reaction. The reactants were mixed into a slurry for 1 h with a magnetic stirrer, moved to a platinum crucible, and heated at 100 °C for 4 h under an argon atmosphere. Then, the temperature was increased to 800 °C and the mixture was held at that temperature for 24 h. Finally, the crucible was cooled to 500 °C at a rate of 2 °C h^{-1} and air quenched to ambient temperature, and the CUP powder of crystals was obtained. To purify the CUP crystals from the unreacted components, the sample has been rinsed in boiling deionized water for 3 times followed by drying in an air-circulated oven at 130 °C.

Solution-casting of PIC membranes.—The PIC membranes were fabricated by means of the low-cost solution-casting technique (Fig. 2) via casting the slurry of the CUP nanoparticles (NPs) that were uniformly dispersed in PBI/DMAc solution with the CUP/PBI mass ratio of 3: 1 (75 wt%). During the process, the desired amount of the CUP powder was ground using a mortar and pestle and then dispersed in DMAc via sonication for 15 min followed by magnetic stirring for 2 h. The desired amount of the PBI-DMAc S26 solution was added into the CUP-DMAc dispersion under vigorous stirring followed by magnetic stirring for 24 h at ambient temperature to form the tri-phase PBI-CUP-DMAc slurry. The final mass fraction of the PBI in the PBI-CUP-DMAc slurry was 18%. Then, the PBI-CUP-DMAc slurry was cast onto a steel panel to form a wet layer with the desired thickness. The as-cast PIC membranes (on the steel panels) were dried in an air-circulating oven at 125 °C for a few minutes to evaporate the sufficient amount of solvent (DMAc) and then rinsed in deionized (DI) water at ambient temperature for peeling off from the steel-panel substrate. Finally, the obtained free-standing PBI-CUP PIC membranes were annealed in the air-circulating oven at 125 °C for another few minutes to form the targeted solution-cast PIC membranes ready for use.

Structural characterization of CUP powder and PIC membranes.—Surface morphologies of the CUP powder and the cross-section of the PIC membranes were characterized by using a field-emission scanning electron microscope (FE-SEM) (JEOL JSM-7600F, JEOL Ltd., Japan). The cross-sectional surfaces of the PIC membrane samples were generated by fracturing the fragile membrane samples after quenching in liquid nitrogen. Prior to SEM characterization, the samples were first sputter-coated with carbon to avoid possible charge accumulation onto the membrane samples during the SEM characterization. In addition, the elemental composition of the CUP samples was analyzed by means of energy-dispersive X-ray spectroscopy (EDS) after the SEM micrographs were taken.

Fourier transform Infrared spectroscopy (FTIR) analysis of CUP powder.—The functional groups of the CUP powder were

characterized by using a Thermo Scientific Nicolet Fourier Transform Infrared Spectrometer (Thermo Fisher Scientific, Waltham, MA). The characterization was performed using the KBr pellet method. During the process, the CUP powder sample was ground with KBr with the mass ratio of $\text{CeP}_5\text{O}_{14}$: KBr = 1: 100 by using an agate mortar and pressed at 2 tons to obtain the disc samples. FTIR spectra were obtained in the wavenumber range of 600–4,000 cm^{-1} with the resolution of 4 cm^{-1} and the CO_2 and H_2O compensation.

X-ray diffraction (XRD) characterization of CUP powder.—Single crystal XRD data were collected using a Kappa Apex II Duo X-ray Diffractometer (Bruker AXS LLC, Madison, WI). A small quantity of the CUP powder sample was used and placed on the diffractometer. The powder sample was kept at 0 °C during the entire data collection process. By using the crystallography software package Olex2 (OlexSys. Ltd., Durham, NC), the crystalline structure was solved using the charge flipping method available in olex2.solve Structure Solution Program and was further refined using the Gauss-Newton minimization method available in olex2.refine Refinement Software Package. Powder XRD characterization was performed at ambient temperature with a Bruker D8 Discover X-ray Diffractometer (Bruker AXS LLC, Madison, WI) by using $\text{Cu-K}\alpha$ radiation. The data for the powder samples were collected for the 2θ values between 0° and 73° with an angular step of 0.005°.

Thermal characterization of CUP powder and PIC membranes.—Thermogravimetric analysis (TGA) was performed by using a thermogravimetric analyzer Q500 (TA Instruments, New Castle, DE) to determine the percent overall mass loss and percent derivative mass loss of the samples with respect to the heating temperature. The tested samples were first heated from ambient temperature (~ 22 °C) to 300 °C at a heating rate of 10 °C min^{-1} and maintained at 300 °C for 1 h. Then, the samples were heated up to 350 °C at the same heating rate of 10 °C min^{-1} and maintained at that temperature for another 1 h. The tests were performed under N_2 and air atmosphere, respectively. For the ramping test, the samples were heated from ambient temperature to 1,000 °C at the heating rate of 10 °C min^{-1} . In addition, dynamic scanning calorimetric (DSC) analysis was carried out by using a Q1000 Modulated Scanning Calorimeter (TA Instruments, New Castle, DE). The experiment was performed for the CUP powder sample in a platinum crucible under N_2 atmosphere with a constant heating rate of 10 °C min^{-1} from 20 to 400 °C.

Mechanical characterization of PIC membranes.—An Instron 5542 tensile tester (the Instron Inc., Norwood, MA) installed with a computerized digital data acquisition system (with the maximum load-carrying capacity of 100 N) was utilized to obtain the tensile stress-strain diagrams of the PIC membranes (with the CUP mass fraction of 75%). The ASTM D882–18 standard test method for tensile properties of thin plastic sheeting was followed in this test.⁵⁷ During the process, the rectangular microtensile test specimens with the areal size of 10 mm × 70 mm and thickness of ~135 μm were scissored cautiously from the PIC membrane samples. Adhesive tabs with the areal size of 10 mm × 10 mm were cut from a 3 M Scotch® foam-mounting double-sided tape and firmly attached onto the two

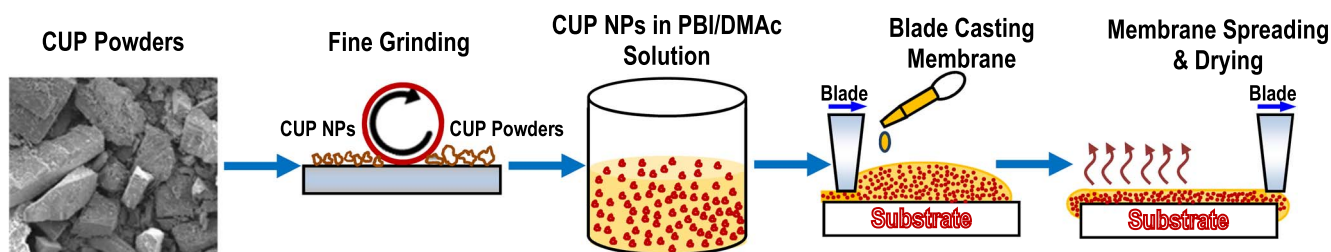


Figure 2. Fabrication route for solution-casting PBI-CUP PIC membranes.

ends at each side of the microtensile test specimen in order to avoid the possible pre-mature failure (brittle cracking) to happen at the fixture regions, in particular in the present case of the seemingly brittle PIC membranes due to the high mass fraction of the CUP particles (up to 75 wt%). Thus, the nominal/effective areal size of the microtensile test specimens of the PIC membrane was 10 mm × 50 mm. During a uniaxial tension test, displacement control with the constant loading rate of 2 mm min⁻¹ was maintained and at least three specimens were tested in each case of the PIC membrane specimens.^{56,58–61} A tension test with the specimen ultimate failure occurring between the upper and lower tabs was considered as a successful test to count, and the corresponding load–displacement diagram was recorded for post-test data reduction to extract the mechanical properties of the specimen. The microtensile test specimens and the microtensile testing setup are shown in Fig. S1 (available online at stacks.iop.org/JES/169/094505/mmedia). For the purpose of comparative study, control microtensile test specimens made of procured PBI films with the thickness of 55 μm (PBI Performance Products Inc., Charlotte, NC) were also prepared following the same procedure above and tested.⁵⁶

Preparation of electrodes and IT-MEAs.—The GDEs were prepared by air-brushing the Pt/C catalyst ink onto the procured gas diffusion layers (GDLs) (the Fuel Cell Store, College Station, TX) as shown in Fig. S2. The catalyst ink was prepared by mixing 30 mg Pt/C catalyst (Pt/C mass ratio of 60: 100, purchased from the Fuel Cell Store, College Station, TX), 2.0 mg of the PBI-CUP suspension (mass ratio CeP₅O₁₄: PBI = 98: 2), and 0.8 g of the solvent carrier of DMAc. The ink was sonicated for 30 min for uniform mixing and then air-sprayed onto the surface of a square-shaped GDL with the areal area of 25 cm². During the air-brushing process, the GDL was placed onto a hot plate at 130 °C to ensure the complete evaporation of the solvent (DMAc). As a result, the GDEs were fabricated with the Pt-catalyst loading of 1.0 mg cm⁻². The IT-MEA was assembled via a hot pressing process. During the process, the five-layered MEA laminate was assembled using a hand lay-up, in which the PIC membrane sample with the areal dimensions of 4 cm × 4 cm was placed in between two GDEs (i.e., the anode and cathode, respectively), each of which carried an active area of 5 cm², and then hot-pressed at the heating temperature of 150 °C and the pressure of 2.5 MPa for 10 min. The thickness of each GDL after hot-pressing was reduced to ~83% of its original thickness. In consequence, the hot-pressed MEA was installed into a single-stack

fuel cell fixture (SAI Cell-525, Scribner Associates Inc., Southern Pines, NC) for hydrogen fuel cell testing.

Single-stack hydrogen fuel cell testing.—A Scribner 850e fuel cell test station (Scribner Associates Inc., Southern Pines, NC) was used to evaluate the electrochemical performance of the fabricated IT-MEA and the proton conductivity of the installed IT-PIC-PEM. The single-stack hydrogen fuel cell was operated under the conditions: $T_{H_2} = T_{Air} = 80$ °C (humidified with the relative humidity of ~47%), $T_{cell} = 200$ °C, back-pressure = 1.0 bar (for both H₂ and air), a minimum mass flow rate of 0.08 l min⁻¹ and the stoichiometry of 1.2 for H₂ as well as 0.15 l min⁻¹ and the stoichiometry of 2.5 for air. Prior to the data acquisition of the fuel cell performance, the IT-MEA was first activated via a break-in procedure at the cell temperature of 200 °C such that the cell had been held via applying a pseudo-cyclic voltage with the alternative amplitudes of 0.6 V, 0.3 V, and then an open circuit condition with the constant duration of 60 s, respectively, for 20 cycles. The break-in procedure can be also beneficial to remove the possible tiny amount of residual DMAc solvent (with the boiling point of 165 °C) in the PIC membrane. The proton conductivity values were extracted from the electrochemical impedance spectroscopy (EIS) measurements, which were conducted on the single-stack hydrogen fuel cell [operated at the constant direct current (DC) density of 0.1 A cm⁻² with 10 steps decade⁻¹ in the frequency range from 0.1 to 10 kHz and the alternative current (AC) with the amplitude of 5% of that of the DC was superimposed onto the DC. The Z-plot was recorded for spectra analysis. The proton conductivity of the PIC PEM was calculated as

$$\sigma \text{ (S/cm)} = \frac{L \text{ (cm)}}{R \text{ (Ohm)} \times A \text{ (cm}^2\text{)}}, \quad [1]$$

where σ (S cm⁻¹) is the proton conductivity of the PIC membrane, L (cm) the membrane thickness, R (ohm) the extracted ionic resistance that was taken from the Nyquist plot, and A (cm²) is the active area of the PIC membrane. During the test, the fuel cell was held at open circuit condition between two consecutive EIS measurements.

Results and Discussion

CeP₅O₁₄ (CUP) characterization.—FTIR analysis was utilized to evaluate the chemical bonds of the synthesized CUP powders from two different batches. Figure 3 shows the identical FTIR

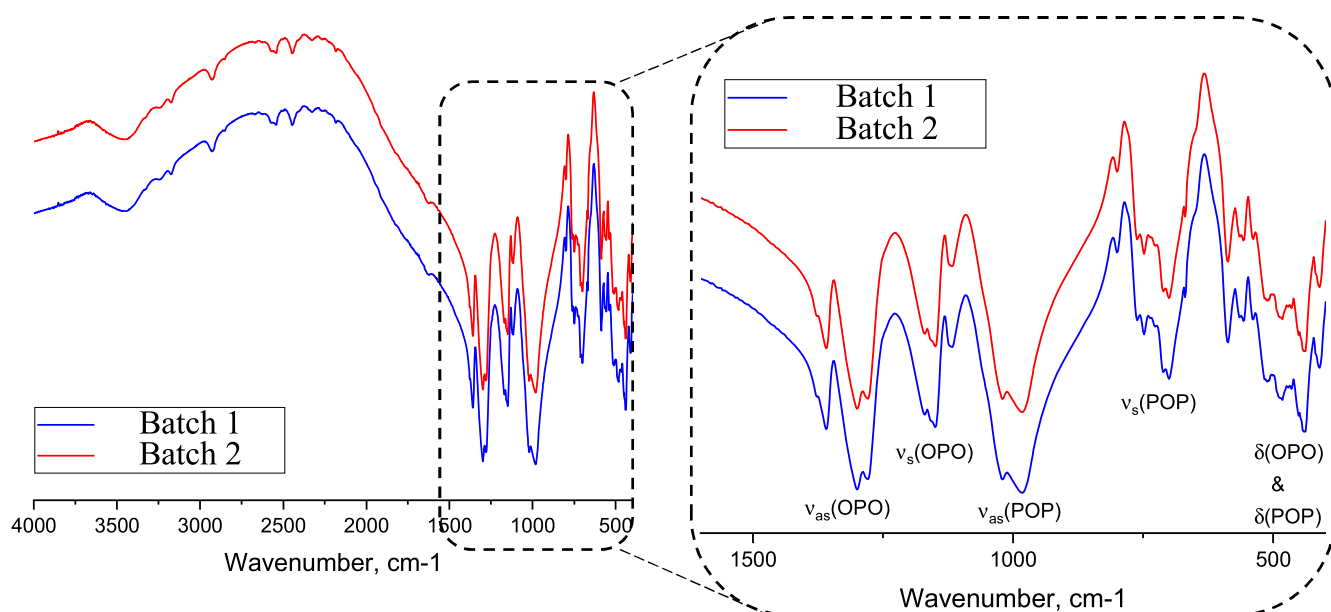


Figure 3. FTIR spectra of CeP₅O₁₄ (CUP) synthesized from two batches.

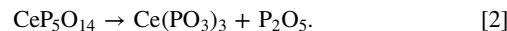
spectra for both synthesized compounds that demonstrate the excellent repeatability of the synthesis process. The absorption peaks occurring between 1,252 and 1,395 cm^{-1} are resulted from the stretching vibrations of ν_{as} (O–P–O), while the vibration bands at 1,150 and 1,170 cm^{-1} are attributed to the deformation vibrations of ν_{s} (O–P–O). The broadband at 807 – 1,090 cm^{-1} is attributed to the ν_{as} (P–O–P) stretching vibrations while the absorption peaks at 670 – 785 cm^{-1} correspond to the deformation vibrations of ν_{s} (P–O–P). Whereas, the absorption peaks at 422 – 534 cm^{-1} are assigned to the bending vibrations of δ (P–O–P) and δ (O–P–O). The appearance of the broadband at 3,458 cm^{-1} and absorption peak at 1,632 cm^{-1} can be attributed to the O–H stretching and bending modes of the adsorbed water molecules.

Accordingly, three possible crystal structures of CUP were reported in the literature,^{48,62–64} i.e., the monoclinic crystal structures with the space group C2/c, the orthorhombic crystal structure with the space group Pnma, and the triclinic crystal structures with the space group P1. Nevertheless, the orthorhombic form was found to be the most stable crystal structure, which can be achieved via crystallization under specific processing conditions. Single-crystal XRD was performed by using a Kappa Apex II Duo X-ray Diffractometer (Bruker AXS LLC, Madison, WI) to evaluate the crystal structure of the synthesized CUP powder (Fig. S3 and Table S1). It was shown that the synthesized CUP crystals are orthorhombic with the Pnma space groups. The powder XRD results provide the information of the CUP crystal structure as well as the purity of the synthesized CUP material (Fig. S4). The spectra of the two samples synthesized from two different batches are the same, indicating the identical crystal structures of the two samples, i.e., orthorhombic. Meanwhile, no additional peaks were detected and, therefore, other types of crystal lattices are not present in the samples. According to the work by Onoda and coauthors,⁶⁵ after grinding for a long period of time, the surface P–O–P bonding in ultraphosphates is expected to convert into P–O–H bonding. However, no differences were detected in the XRD spectra of the samples before and after grinding with the mortar and pestle in the present study. As a result, the crystal structure of the CUP powder remained the same from batch to batch and after the grinding process, which indicates the high reproducibility of the CUP synthesis process.

Figure 4 shows the SEM micrographs of as-synthesized and ground CUP powder samples in term of polydisperse particles. In addition, grinding did not noticeably alter the morphological and crystalline structures of the as-synthesized CUP particles. Furthermore, to verify the elemental composition of the as-synthesized CUP powder, SEM-EDS was further utilized for characterization (Fig. S5). Table I summarizes the elemental composition of the CUP powder sample, which shows that the mass concentrations of elements of cerium (Ce) and phosphorus (P) are slightly below the theoretical calculations (below 4%) while the mass concentration of oxygen (O) is around 6% higher than the theoretical prediction. The experimental results of the molar ratio of P over O are also 4%–8% below the theoretical prediction ($5/14 = 0.35714$). The difference between the experimental measurements and theoretical predictions could be induced by the atomic number effect and is within the range of device accuracy. In addition, no impurities of other elements were detected, indicating the high purity of the as-synthesized CUP powder.

Thermal analysis of CUP.—Thermogravimetric analysis (TGA) was utilized to evaluate the thermal stability of the as-synthesized CUP powder. Figure 5 shows the thermogravimetric behaviors of the CUP powder samples that were tested respectively under air and nitrogen atmospheres under the ramp heating up to 1,000 °C. In both cases, the CUP powder samples remained stable until ~800 °C. The mass loss of the CUP sample that was tested under a nitrogen atmosphere at 810 °C is ~0.43%, while tested in the air at 840 °C, the mass loss of the CUP sample is ~0.22%. The present results are in a good agreement with the data reported by Szczygiel and

Znamierowska,⁴⁸ who indicated that CUP is unstable at higher temperatures (above 900 °C) and decomposes according to the reaction:



The mass decrement on the TGA curves above 810 °C – 840 °C can be attributed to the evaporation loss of P_2O_5 . Figure 6 shows the thermogravimetric behaviors of the CUP powder samples in different atmospheres (air and nitrogen) by heating the samples to a specified temperature (300 and 350 °C in sequence) and then holding the samples at this temperature for 1 h. The overall mass loss of the sample under nitrogen atmosphere was found as ~0.25% while it was ~0.50% in the air. The TGA results indicate the high thermal stability of the as-synthesized CUP powder samples.

Differential scanning calorimetric (DSC) characterization provides the information about the phase transition and thermal effects that occur in the course of the heating process according to the peaks of heat absorption and emission rates with respect to the heating temperature (e.g., exothermic or endothermic, narrow or wide, etc.). The appearance of the exothermic peak of heat absorption or emission can correspond to the changes of the crystal structures of the solid-state proton conductor (e.g., from hexagonal to monoclinic), while the presence of the broad peak can be attributed to the transition from amorphous to crystalline structures.⁶⁶ It is reported that rare-earth ultraphosphates can undergo the second-order phase transition from monoclinic to orthorhombic crystal structures in the temperature range from 117 to 180 °C, and the transition temperature rises with increasing lanthanide atomic number.^{67–70} Figure S6 shows the DSC data of the CUP powder sample. The exothermic peak at ~200 °C can be attributed to the phase transition during the heating process. To investigate the changes in the CUP crystal structure, XRD data were recorded using an XRD analyzer equipped with a heated stage (Figs. S7 and S8). During the process, the CUP particles were mounted on the stage and the temperature was controlled to ramp up from ambient temperature to 600 °C and then down to ambient temperature with the temperature interval of 30 °C. The XRD patterns were acquired at each sampling temperature with the increment of 30 °C under the humidified nitrogen atmosphere. These figures indicate that the orthorhombic crystal structure with the Pnma space groups was the only crystal structure of the as-synthesized CUP powder, and there are no noticeable impacts of the high temperature and steam on the CUP crystallinity or composition.

PBI-CUP PIC membrane characterization.—Solution-casting is a low-cost, scalable membrane processing technique that is utilized for the preparation of the present PIC membrane samples. Our studies show that the solution-casting technical can be conveniently used for producing high-quality PBI-CUP PIC membranes (with uniform thickness and without pinholes and obvious roughness) with the CUP mass fraction of up to 85% (Fig. S9). With the addition of the CUP particles, the gloss of the membranes decreases and the membrane surfaces become rougher. In principle, the size and distribution of the CUP particles within the polymer matrix play an important role in the electrochemical, physical, and mechanical properties of the resulting PIC membranes. As a matter of fact, PBI membranes without acid-doping exhibit nearly negligible proton conductivity while the CUP particles carry the high proton conductivity. In the PBI-CUP PIC membranes, CUP particles function as the solid-state proton conductor while PBI functions as a polymeric binder. To achieve the high proton conductivity of the PBI-CUP PIC membranes, reasonably high mass fraction of the CUP particles is expected with the compromise of the resulting mechanical properties and structural integrity. Figure 7 shows the SEM micrographs of the cross-sections of the solution-cast PBI-CUP PIC membranes containing 75 and 85 wt% of CUP, respectively, in which the CUP particles can be clearly distinguished. In the case of the PIC membrane with 75 wt% of CUP, uniform

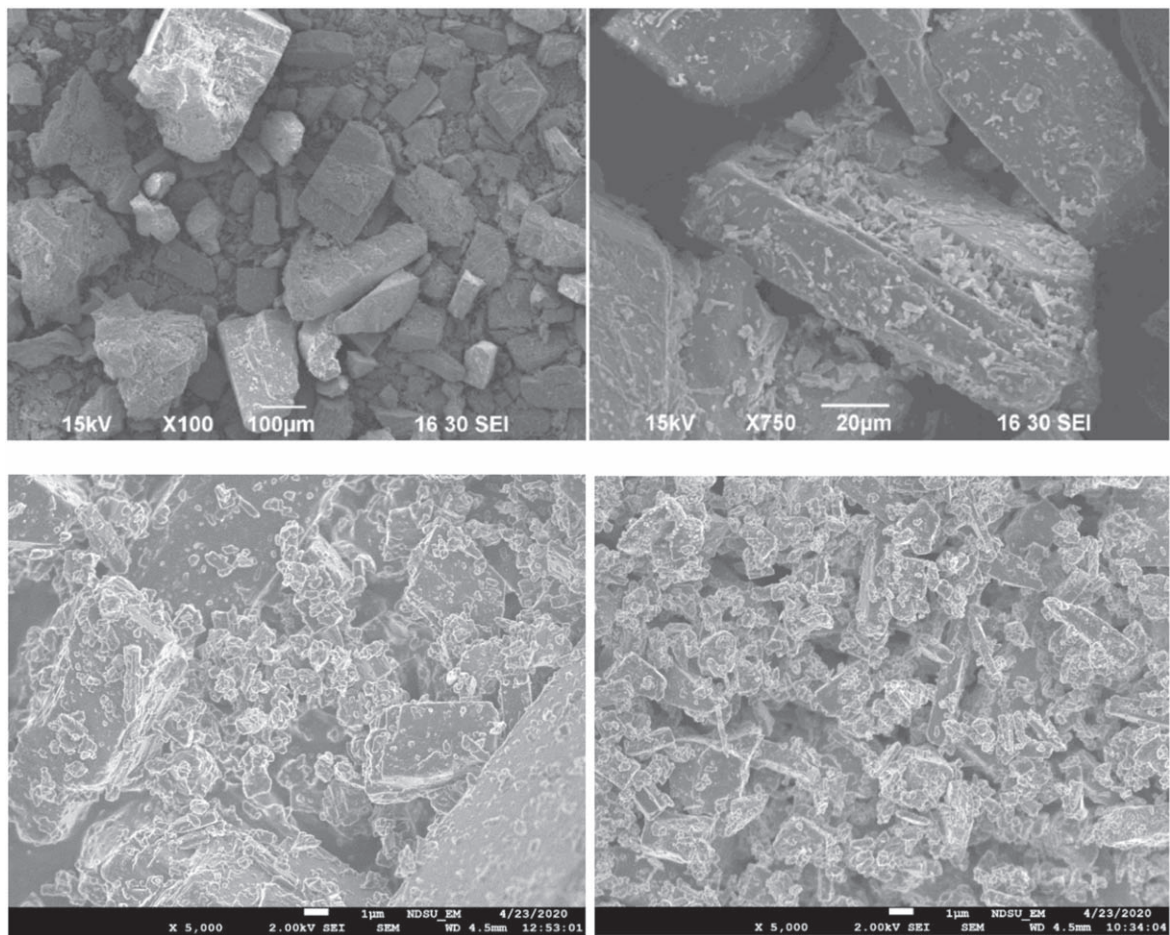


Figure 4. SEM micrographs of as-synthesized (top) and ground (bottom) CUP powder samples.

Table I. Quantitative element composition of the CUP powder sample.

Element composition	Elements		
	O	P	Ce
Experimental measurement (wt%)	45.88 ± 0.87	29.10 ± 0.71	25.02 ± 1.56
Theoretical prediction (wt%)	43.16	29.84	27.00

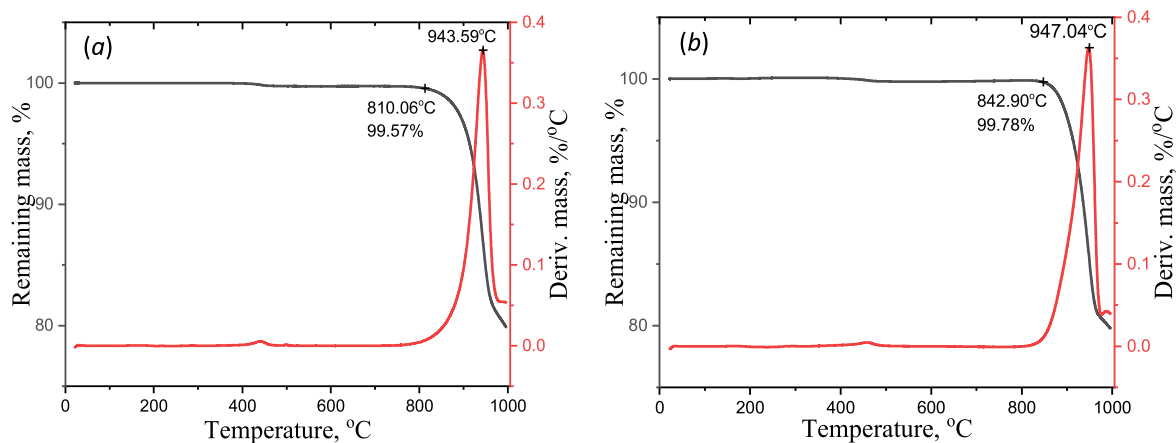


Figure 5. TGA-based thermal stability assessment of the CUP powder sample under ramp heating. (a): Tested in nitrogen; (b): Tested in air.

distribution of the CUP particles can be observed. Yet, in the case of

the PIC membrane with 85 wt% of CUP, obvious cavities and pores

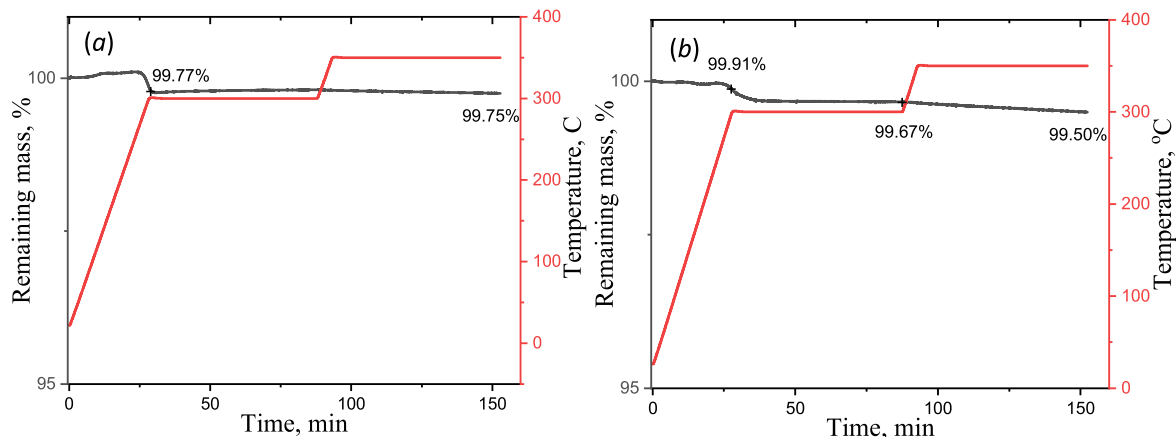


Figure 6. TGA-based thermal stability assessment of the CUP powder sample. (a): Tested in nitrogen; (b): Tested in air.

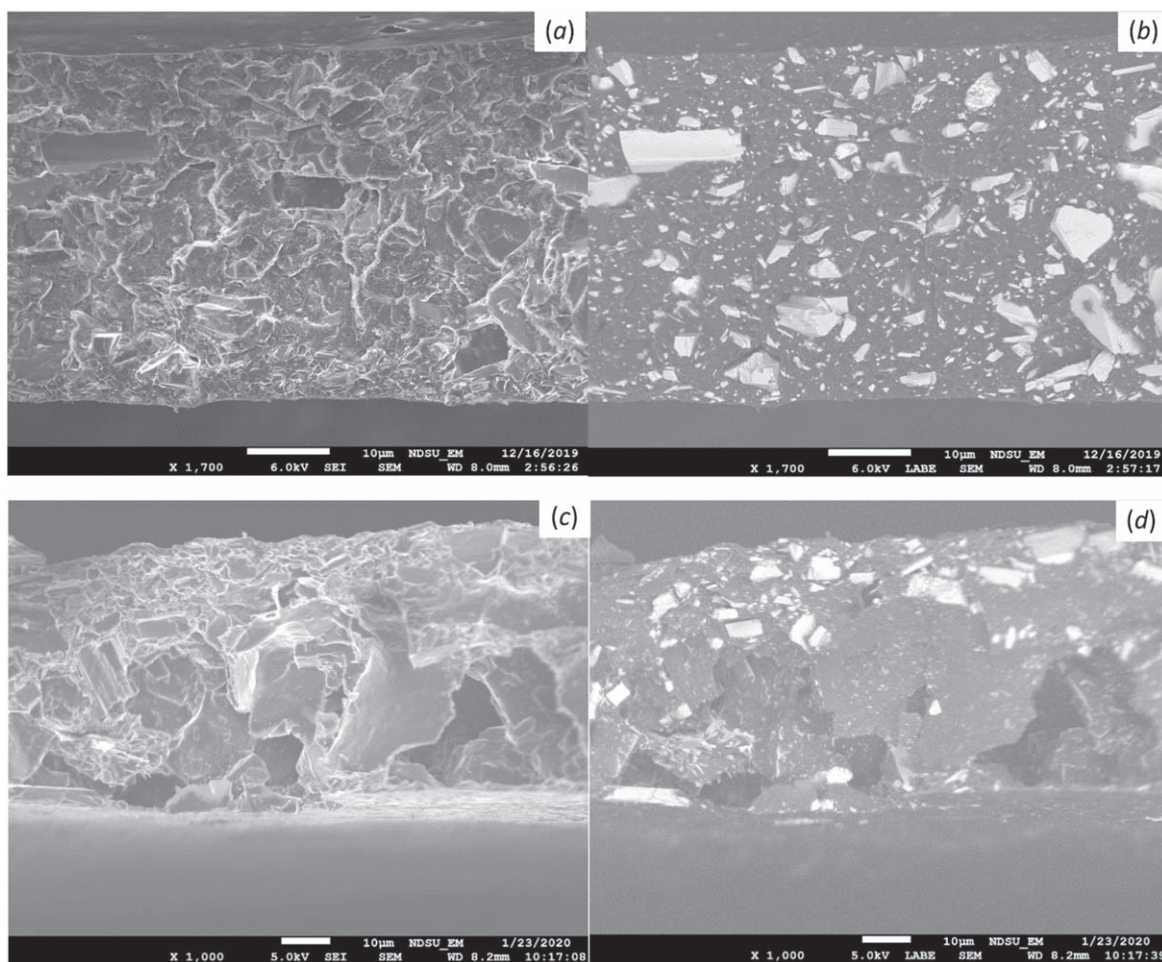


Figure 7. SEM micrographs of the cross-sectional morphologies of the solution-cast PBI-CUP PIC membrane samples. (a) & (b): With 75 wt% of CUP; (c) & (d): With 85 wt% of CUP. (a) & (c): Secondary electron imaging; (b) & (d): Backscattered imaging.

can be found in the membrane cross-section due to the high amount of the inorganic material (CUP). Thus, only PIC membranes with 75 wt% of CUP were selected in the present study for fabrication and characterization of the IT-MEAs to ensure the structural integrity and high CUP mass fraction of the resulting PIC membranes for high proton conductivity and high durability of the electrochemical, physical and mechanical properties.

Elemental EDS analysis was conducted at the typical cross section of the PIC membrane as shown in Fig. 8 and confirmed

that the presence of elements of Ce and P was from the CUP particles while elements of C and N are related to the PBI. In addition, element O can be attributed to both the CUP and PBI as the organic and inorganic constituents of the PIC membranes. Table II summarizes the EDS results of the cross-sections of the PIC membrane samples with 75 and 85 wt% of CUP, respectively. In the case of the PIC membrane sample with 75 wt% of CUP, the CUP distribution across the thickness is nearly even. In contrast, in the case of 85 wt% of CUP, the CUP distribution across the membrane

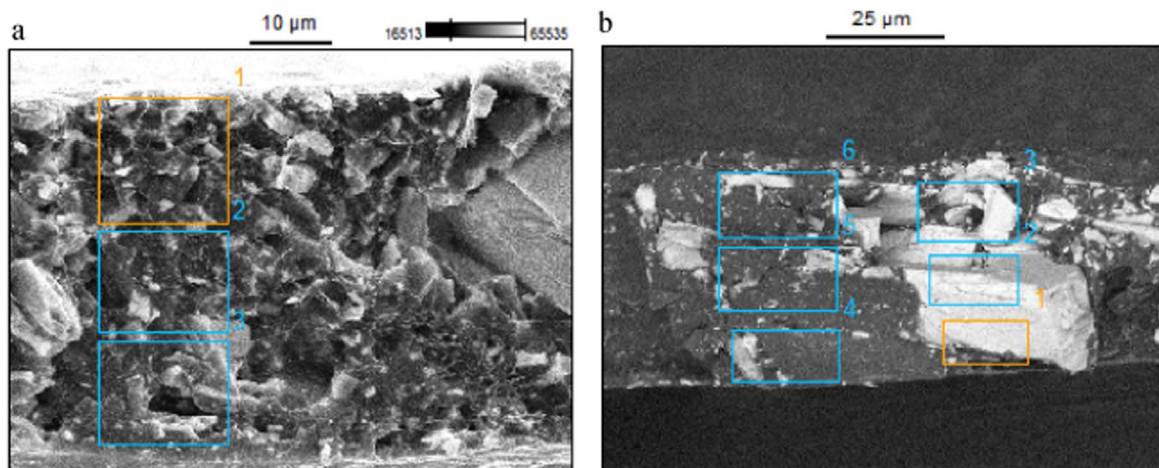


Figure 8. EDS of the cross-sections of solution-cast PBI-CUP PIC membranes. (a): With CUP mass fraction of 75%, (b): With CUP mass fraction of 85%.

Table II. Quantitative element composition of the PBI-CUP PIC membranes.

CUP mass fraction	Location of sampling point in membrane	Element composition (wt%)				
		C	N	O	P	Ce
75%	Top	41.48 ± 1.27	7.84 ± 4.57	20.87 ± 1.39	13.85 ± 0.43	14.52 ± 1.49
	Middle	35.51 ± 1.21	6.68 ± 2.78	23.93 ± 1.39	15.86 ± 0.42	16.04 ± 1.70
	Bottom	33.84 ± 1.15	6.64 ± 2.64	24.06 ± 1.35	15.69 ± 0.49	18.41 ± 1.76
85%	Top	38.33 ± 1.58	13.15 ± 6.83	33.77 ± 3.75	14.75 ± 2.83	
	Middle	6.10 ± 0.16		30.19 ± 0.73	22.19 ± 1.05	41.52 ± 6.36
	Bottom	5.10 ± 0.19		28.24 ± 0.85	27.16 ± 1.44	39.50 ± 7.93

thickness is much more uneven. Such uneven distribution of CUP can be related to the nonhomogeneous distribution of the CUP particles within the membrane and cavitation in the PIC membrane as evidenced in the SEM micrographs.

Figure 9 shows the thermogravimetric behaviors of the PBI-CUP PIC membrane samples with 75 and 85 wt% of CUP, respectively. During the TGA tests, the PIC membrane samples were heated up to 300 or 350 °C at a ramp heating rate of 10 °C min⁻¹ and then held at this temperature for 1 h. The TGA results indicate that the PIC membrane with 75 wt% of CUP and 25 wt% of PBI contained ~3.35 wt% of moisture and underwent an overall mass loss of ~5.49% in the entire thermogravimetric analysis. Thus, by excluding the moisture loss, the net mass loss of the PIC membrane sample (with 75 wt% of CUP) was ~2.14% due possibly to the evaporation of residual DMAc (with the boiling point of 165 °C), additional bonded water and decomposition of other LT and IT impurities, which demonstrated the high thermal stability of the PIC membrane. In the case of the PIC membrane sample with 85 wt% of CUP, the overall mass loss during the TGA test was ~3.30%, of which ~1.72% belonged to the moisture content. In principle, the lower amount of moisture can be attributed to the lower polymer content in these PIC membrane samples since the CUP particles behave no obvious water absorption according to the TGA test results above (Figs. 5 and 6).

Figure 9c shows the TGA diagram of the typical PIC membrane sample (with 75 wt% of CUP) after proton conductivity measurement, which indicates the similar thermogravimetric performance as that prior to the measurement. In this case, the PIC membrane sample lost ~4.48% of its initial mass during the entire thermogravimetric testing procedure, of which ~1.66% was related to the moisture content in the sample. In addition, the amount of moisture in the PIC membrane sample prior to the proton conductivity test is higher than that after the test, i.e., from 3.35% prior to the proton conductivity measurement down to 1.66% after the test.

Furthermore, in the view of thermal stability of the IT-PIC-PEMs in PEMFC applications, CUP is a thermally stable heavy metal ultraphosphate salt that is synthesized via HT solution reaction at 800 °C and does not dissolve into water or water stream at 200 °C. Yet, physical and chemical degradation of the amorphous m-PBI could happen under attack of radicals at high temperature during the operation of the IT-PEMFCs, especially at the interfaces between the CUP particles and PBI, which cannot be validated simply through the TGA test. Technologically, the durability of amorphous PBIs such as the typical m-PBI adopted in this work can be improved via crosslinking.^{28–32}

Mechanical characterization of PBI-CUP PIC membranes.—

The ultimate tensile strengths and tensile strains at break of the present PBI-CUP PIC membranes, solution-cast pure PBI membranes as well as the procured PBI films (PBI Performance Products Inc., Charlotte, NC) are tabulated in Table III. These data are extracted from the stress-strain diagrams of the PIC membrane samples (with 75 wt% of CUP) and the control film samples of the solution-cast PBI membranes (Fig. S10). With 75 wt% of CUP, the PIC membranes behaved brittle with the average tensile strength of 5.79 MPa (comparable to those of low-strength polymers) and the average tensile strain at break of 2.68%, both of which are much lower than those of the solution-cast pure PBI membranes and procured PBI films. In addition, the initial modulus of the PIC membranes is estimated from the stress-strain diagrams as ~400 MPa, which is ~1/5 that of the solution-cast pure PBI membranes. Though the PIC membrane carried much lower tensile strength and tensile modulus compared to those of pure PBI membranes, it is mechanically flexible (Fig. S8) and suitable for use as PEMs in IT electrochemical processes where the PEMs do not carry the tensile loads. The PBI-CUP PIC membranes with 85 wt% of CUP was eliminated from the mechanical and further electrochemical characterizations due to their uneven distribution of the

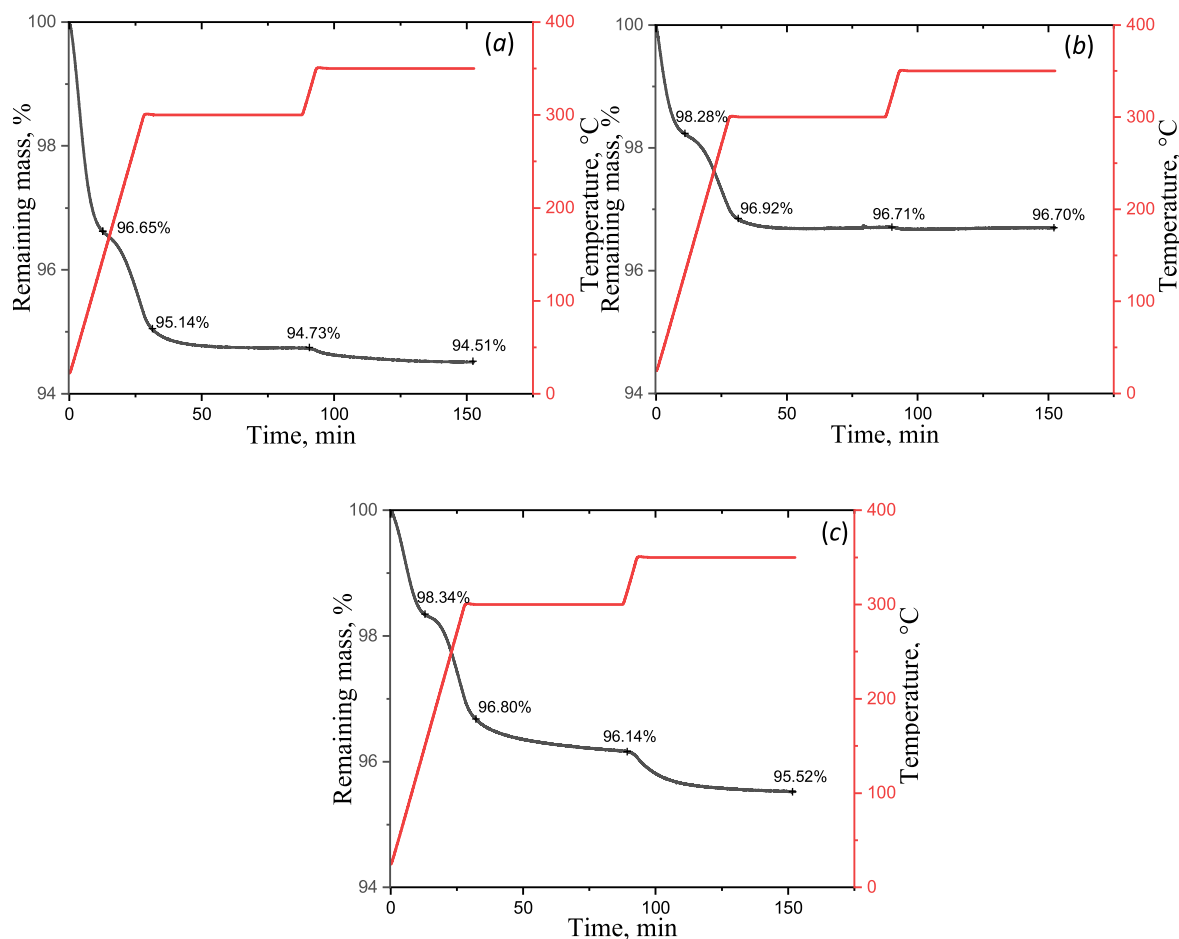


Figure 9. TGA and DTG diagrams of the PBI-CUP PIC membrane samples. (a): With 75 wt% of CUP; (b) with 85 wt% of CUP; (c) with 75 wt% of CUP after proton conductivity measurement.

Table III. Ultimate tensile strength and tensile strain at break of the PBI films and PBI-CUP PIC membrane samples.

Sample	Commercial PBI film	Solution-cast PBI	PBI-CUP PIC membrane (CUP: 75 wt%)
Tensile strength (MPa)	130.08 ± 17.03	120.35 ± 16.54	5.79 ± 0.91
Tensile strain at break (%)	9.81 ± 0.68	6.71 ± 0.47	2.68 ± 0.48

CUP particles and visible cavities (poor structural integrity) within the membrane cross-sections.

Proton conductivity measurement of PBI-CUP PIC membranes.—Figure 10 shows the variation of the measured proton conductivity of a typical PBI-CUP PIC membrane (with 75 wt% of CUP) with the testing time within the first 500 h after the electrochemical break-in procedure for one hour. The values of the proton conductivity are extracted from the Nyquist plots as shown in Fig. 10a, which were measured from the IT-MEA during the single-stack hydrogen fuel cell test under constant electrical current load of 0.1 A cm^{-2} at $200 \text{ }^\circ\text{C}$ by using the Scribner® 850e fuel cell test station. As observed from Fig. 10a, the high- and low-frequency intercepts with the real axis decrease after a couple of hours of the fuel cell test, and the low-frequency intercept is in coincidence with that measured after 13 h of the fuel cell test while the high-frequency intercept is lower than the corresponding intercept measured after 13 h of the fuel cell test. The diameter and intercepts of the curves remain the same until about 400 h of the fuel cell test, then the diameter and the low-frequency intercept with the real axis slightly decrease. However, the change in the high-frequency intercept is negligible. This possibly indicates that the PIC membrane sample

became fully hydrated by the moisture generated in the cell after about 13 h of the fuel cell test and remained hydrated during the entire test, i.e., the proton conductivity of the PIC membrane in the IT-PEMFC is closely related to its water content.⁷¹ Meanwhile, the mass transfer resistance decreased, resulting in the decrease of the low-frequency intercept with the real axis. The proton conductivity measurements were performed after the break-in procedure. It needs to be mentioned that the present PIC membrane could still contain a tiny amount of residual DMAc solvent (the boiling point of $165 \text{ }^\circ\text{C}$) with strong interaction with the PBI even after 1 h of the electrochemical break-in procedure at $200 \text{ }^\circ\text{C}$. The possible further release of the residual DMAc solvent out of the PIC membrane at the beginning of the fuel cell test at $200 \text{ }^\circ\text{C}$ might also have slightly contributed to the growing proton conductivity. Additional experimental effort can be made to eliminate the tiny residual DMAc solvent after solution-casting to suppress such effect such as drying and annealing the PIC membranes at $200 \text{ }^\circ\text{C}$ and rinsing in boiling water. Furthermore, Fig. 10b shows that the value of the proton conductivity of the present PIC membrane grew up with the time from 2.0×10^{-2} to $5.8 \times 10^{-2} \text{ S cm}^{-1}$ and reached the plateau value of $5.8 \times 10^{-2} \text{ S cm}^{-1}$ within approximately 13 h of the fuel cell test. Furthermore, no decreasing trend in the proton conductivity value

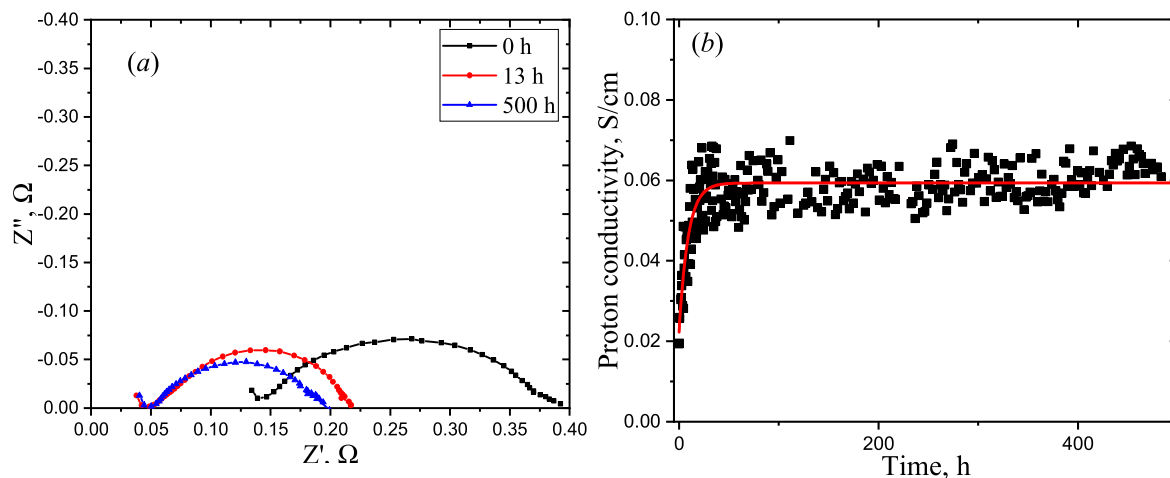


Figure 10. (a) Nyquist plots of the EIS characterization of a typical MEA made of the PBI-CUP PIC membrane (with 75 wt% of CUP) at 200 °C; (b) variation of the measured proton conductivity of the IT-MEA with the testing time from 0 to 500 h (Symbols: Sampling data points; solid curve: Fitting curve of the average values of proton conductivity).

was noticed within 500 h in the present test. Such high values of the proton conductivity of the present PIC membrane at 200 °C are comparable to those of LT Nafion® membranes at the fully hydrated state, which indicates the successful fabrication of the GDEs of the IT-MEA used for the present electrochemical characterization. Figure 11 shows the SEM micrograph of the typical surface morphology of the catalyst layer of the GDE to evidence the well porous microstructures, and Fig. 12 shows the EDS elemental mapping results of the catalyst layer to indicate the even distribution of the catalyst Pt and CUP NPs on the surface of the catalyst layer.

The initial performance data of the IT-PEMFC installed with the present PBI-CUP PIC membrane was investigated. Figure 13 represents the typical polarization curve ($V-I$ diagram) and power density curve ($P-I$ diagram) of the IT-PEMFC that was operated at 200 °C with humidified hydrogen and air. The IT-MEA provided the open circuit voltage (OCV) of 0.87 V (with the membrane thickness of 135 μm) with the maximum power density of 115 mW cm^{-2} . In addition, the maximum current (~ 2.70 A) is close to theoretical estimate based on the air flow of 150 ml min^{-1} at the stoichiometry of 2.5, which corresponds to an overall current of 3.6 A. In principle, various factors can influence the voltage reduction of the IT-PEMFC during the test, e.g., ionic and electrical resistances, electrochemical reaction kinetics, reactant transport limitations to active catalyst sites, etc. Thus, the polarization $V-I$ diagram depends upon multiple factors including the GDLs, microporous layers, PIC membrane,

catalyst layers, operating temperature, gas pressure and humidity, reactant flow rates, flow field design of bipolar plates, etc.²² In addition, for the present IT-PIC-PEMs, the degradation becomes more complicated due to the involvement of the interaction between the two constituents, i.e., the CUP and PBI, and additional microstructure failure modes of the PIC membranes may also include interfacial cracking and cavitation between the CUP particles and PBI as well as intra-grain cracking of the CUP particles, among others. Additional research efforts are expected to explore the fundamental degradation mechanisms of this type of IT-PIC-PEMs. Therefore, multiple technical options can be considered to optimize the material and process parameters of the PIC membranes and the IT-MEAs in order to achieve the maximum electrochemical performance of the resulting IT-PEMFCs.

Conclusions

A rational route has been formulated in this study for successful synthesis and characterization of a new type of IT-PIC-PEMs that were made of cerium ultraphosphate ($\text{CeP}_5\text{O}_{14}$) as the solid-state proton conductor composited with an HT polymer (i.e., m-PBI) as the polymeric binder. In the process, an HT solution reaction has been employed for the synthesis of the CUP powder of crystals, which carried the high-purity orthorhombic crystal structure and demonstrated the high thermal stability with the decomposition temperature up to 810 °C – 820 °C under either nitrogen or air

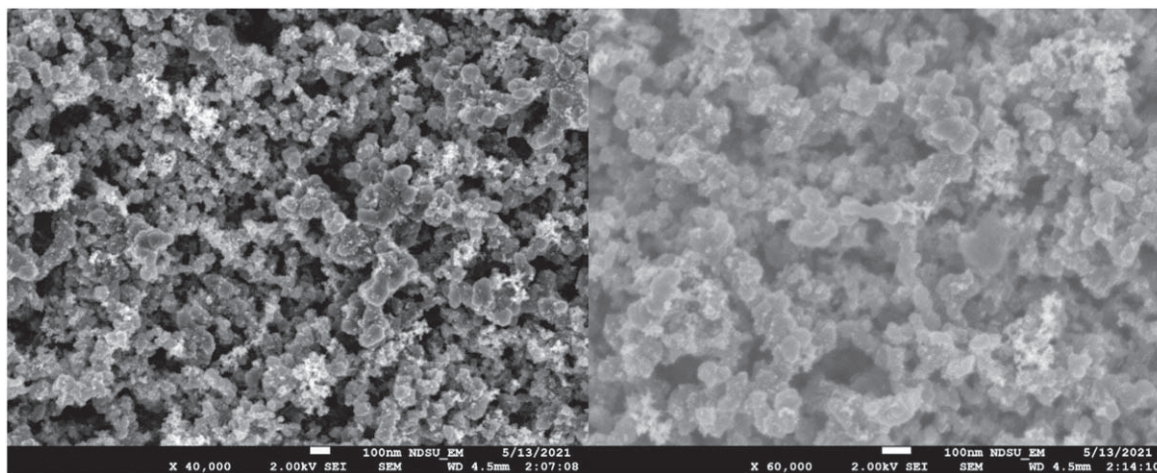


Figure 11. SEM-based surface morphology characterization of the GDE made from the procured GDL with deposited Pt/C nanoparticles on the top (the diameter of Pt NPs: ~ 5 nm).

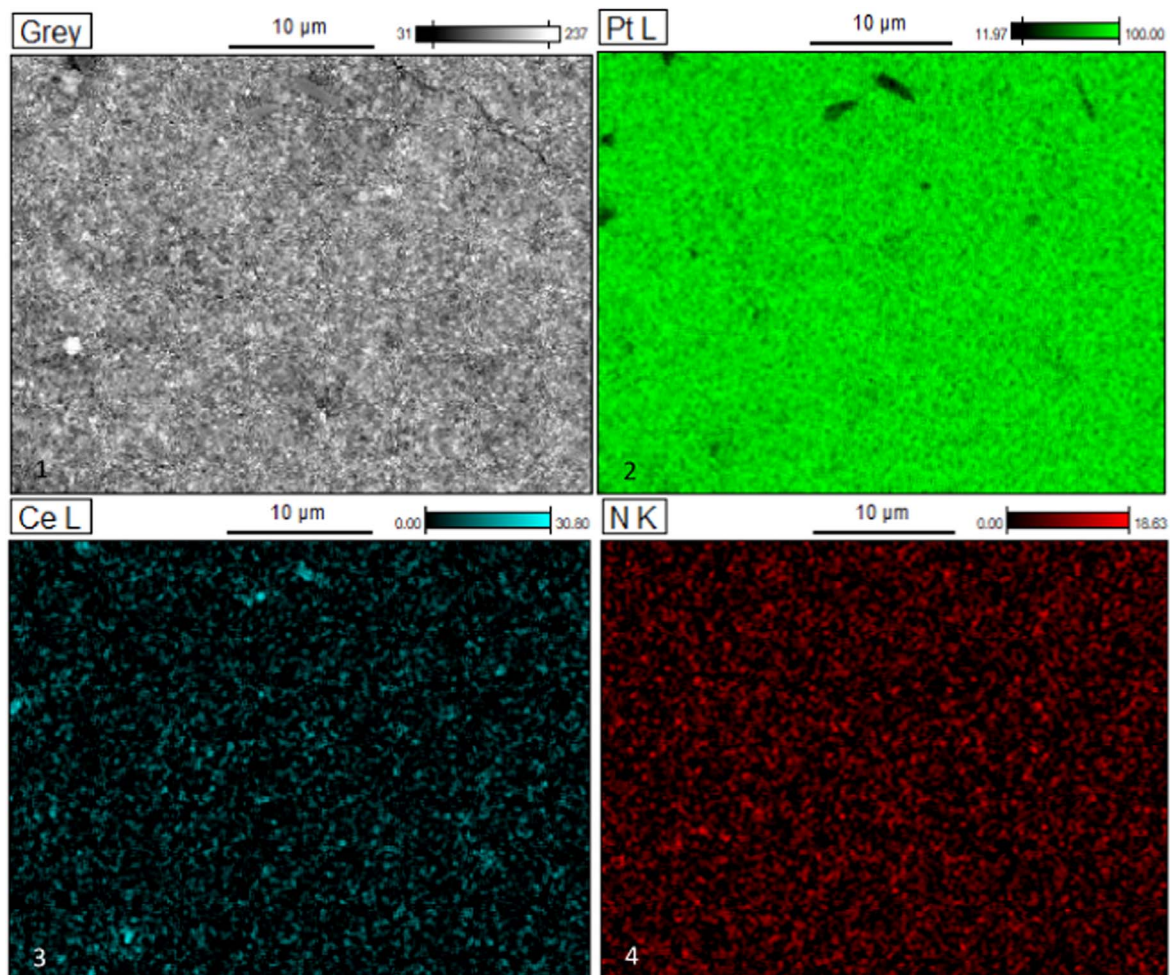


Figure 12. EDS elemental mapping (general and by elements) of the surface morphology of the GDE made of a procured GDL air-brushed with Pt/C and CUP NPs on the top.

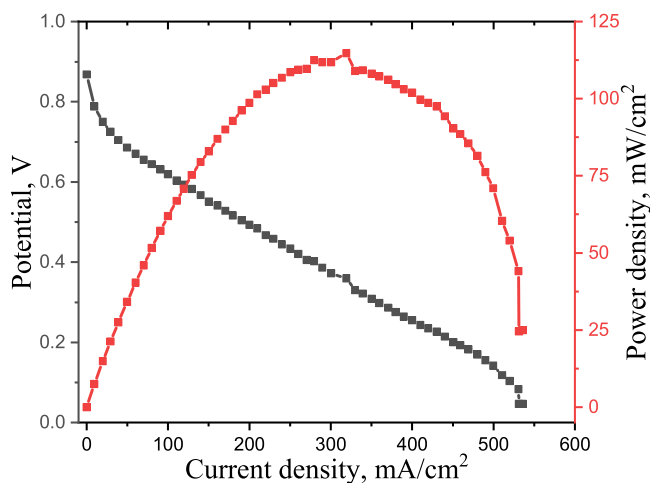


Figure 13. Performance of the prototype IT-PEMFC operated at 200 °C. The active electrode area is 5 cm² with the Pt-catalyst loading of 1.0 mg cm⁻² in both anode and cathode.

atmosphere. The low-cost solution-casting technique has been utilized for fabrication of the mechanically flexible PBI-CUP PIC membranes (with the thickness of $\sim 135 \mu\text{m}$) with the CUP mass fraction as high as 75%. The present study has evidenced that this type of PIC membranes carried high thermal stability at the testing

temperatures of up to 300 to 350 °C under either nitrogen or air atmosphere, high structural integrity, and high proton conductivity of up to $5.8 \times 10^{-2} \text{ S cm}^{-1}$ when operated on a single-stack hydrogen fuel cell under a humidified atmosphere at 200 °C. The measured proton conductivity of the present PBI-CUP PIC membranes showed a very good durability within the initial test duration of 500 h. The preliminary test results of the present study quest additional full-spectrum experimental and theoretical investigations of this type of PIC PEMs for the promising broad uses in various IT electrochemical energy conversion processes including IT-PEMFCs, electrolytic ammonia production, hydrogen separation, electrolysis, membrane-based electrochemical synthesis of valuable chemicals, etc. In particular, additional research efforts are expected to optimize the material and process parameters for the optimal electrochemical performance of the IT-PIC-PEMs and to evaluate their long-term structural integrity as well as electrochemical and mechanical durability under various loading conditions.

Acknowledgments

The financial support of this research by the Office of Energy Efficiency and Renewable Energy (EERE) of the U.S. Department of Energy under the Advanced Manufacturing Office (Award No.: DE-EE0008324) and the Renewable Energy Program of the Industrial Commission of North Dakota (Award No.: R-036-45) is gratefully acknowledged. The views and opinions of authors expressed herein do not necessarily state or reflect those of the United States Government, the Industrial Commission of North Dakota, the EERC, or any agency thereof. The study at North Dakota State

University (NDSU) was also financially sponsored by the ND EPSCoR (Award No.: FAR0031220), ND Corn Utilization Council (Award No.: FAR0032332), and NDSU Development Foundation (Award No.: FAR0031220).

ORCID

Xiang-Fa Wu  <https://orcid.org/0000-0003-2008-7564>

References

- <http://energy.gov/eere/fuelcells/fuel-cells>.
- B. C. H. Steele and A. Heinzel, *Nature*, **414**, 345 (2001).
- I. A. Amar, R. Lan, T. G. Petit, and S. Tao, *J. Solid State Electrochem.*, **15**, 1845 (2011).
- J. N. Renner, L. F. Greenlee, A. M. Herring, and K. E. Ayers, *Electrochem. Soc. Interface*, **24**, 51 (2015).
- V. Kyriakou, I. Garagounis, A. Vourros, E. Vasileiou, and M. Stoukides, *Joule*, **4**, 142 (2019).
- O. Elishav, B. M. Lis, E. M. Miller, D. J. Arent, A. Valera-Medina, A. G. Dana, G. E. Shter, and G. S. Grader, *Chem. Rev.*, **120**, 5352 (2020).
- J. W. Phair and S. P. S. Badwal, *Ionics*, **12**, 103 (2006).
- Z. Tao, L. Yan, J. Qiao, B. Wang, L. Zhang, and J. Zhang, *Prog. Mater. Sci.*, **74**, 1 (2015).
- K. Ayers, N. Danilovic, R. Ouimet, M. Carmo, B. Pivovar, and M. Bornstein, *Annu. Rev. Chem. Biomol. Eng.*, **10**, 219 (2019).
- M. Marony (ed.), *Proton-conducting Ceramics: From Fundamentals to Applied Research*. (Pan Standord Publishing, Singapore) (2016).
- O. Knauth and M. L. di Vona, *Solid State Proton Conductors: Properties and Applications in Fuel Cells*. (Wiley, Wst Sussex, UK) (2012).
- P. Colomban (ed.), *Proton Conductors: Solids, Membranes and Gels-Materials and Devices*. (Cambridge University Press, Cambridge, UK) (1992).
- M. A. Hickner, H. Ghassemi, Y. S. Kim, B. R. Einsla, and J. E. McGrath, *Chem. Rev.*, **104**, 4587 (2004).
- H. Zhang and P. K. Shen, *Chem. Rev.*, **112**, 2780 (2012).
- R. Borup et al., *Chem. Rev.*, **107**, 3904 (2007).
- F. N. Büchi, M. Inaba, and T. J. Schmidt (ed.), *Polymer Electrolyte Fuel Cell Durabilit.* (Spring, New York, NY) (2009).
- E. D. Wachsman and K. T. Lee, *Science*, **334**, 935 (2011).
- M. Liu, M. E. Lynch, K. Blinn, F. M. Alamgir, and Y. M. Choi, *Mater. Today*, **14**, 534 (2011).
- N. Mahato, A. Banerjee, A. Gupta, S. Omar, and K. Balani, *Prog. Mater. Sci.*, **72**, 141 (2015).
- K. Scott, C. Xu, and X. Wu, *WIREs Energy Environ.*, **3**, 24 (2014).
- T. Xiao, R. Wang, Z. Chang, Z. Fang, Z. Zhu, and C. Xu, *Prog. Natl. Sci.: Mater. Int.*, **30**, 743 (2020).
- Q. Li, D. Aili, H. A. Hjuler, and J. O. Jensen (ed.), *High Temperature Polymer Electrolyte Membrane Fuel Cells: Approaches, Status, and Perspectives*. (Spring, Heidelberg, Germany) (2016).
- Q. Li, J. Q. Jensen, R. F. Savinell, and N. J. Bjerrum, *Prog. Polym. Sci.*, **34**, 449 (2009).
- Z. Zhou, O. Zholobko, X. F. Wu, T. Aulich, J. Thakare, and J. Hurley, *Energies*, **14**, 135 (2021).
- K. D. Kreuer, *Chem. Mater.*, **8**, 610 (1996).
- Y. L. Ma, J. S. Wainright, M. H. Litt, and R. F. Savinell, *J. Electrochem. Soc.*, **151**, A8 (2004).
- D. Aili, D. Henkensmeier, S. Martin, B. Singh, Y. Hu, J. O. Jensen, L. N. Cleemann, and Q. Li, *Electrochem. Energy Rev.*, **3**, 793 (2020).
- Y. Oono, A. Sounai, and M. Hori, *J. Power Sources*, **210**, 366 (2012).
- T. Søndergaard, L. N. Cleemann, H. Becker, D. Aili, T. Steenberg, H. A. Hjuler, L. Seerup, Q. Li, and J. O. Jensen, *J. Power Sources*, **342**, 570 (2017).
- Y. Wang, P. Sun, Z. Li, H. Guo, H. Pei, and X. Yin, *ACS Sustainable Chem. Eng.*, **9**, 2861 (2021).
- H. Guo, Z. Li, Y. Lv, H. Pei, P. Sun, L. Zhang, W. Cui, X. Yin, and H. Hui, *ACS Appl. Energy Mater.*, **4**, 8969 (2021).
- H. Guo, Z. Li, H. Pei, P. Sun, L. Zhang, P. Li, and X. Yin, *J. Membrane Sci.*, **644**, 120092 (2022).
- R. He, Q. Li, G. Xiao, and N. J. Bjerrum, *J. Membr. Sci.*, **226**, 169 (2003).
- D. A. Boysen, T. Uda, R. I. Chisholm, and S. M. Haile, *Science*, **303**, 68 (2004).
- J. Otomo, N. Minagawa, C. J. Wen, K. Eguchi, and H. Takahashi, *Solid State Ionics*, **156**, 357 (2003).
- T. Uda and S. Haile, *Solid-State Lett.*, **8**, A245 (2005).
- C. R. I. Chisholm and S. M. Haile, *Mater. Res. Bull.*, **35**, 999 (2000).
- A. Goñi-Urtiaga, D. Presvytes, and K. Scott, *Int. J. Hydrogen Energy*, **37**, 3358 (2012).
- Y. Jin, Y. Shen, and T. Hibino, *J. Mater. Chem.*, **20**, 6214 (2010).
- Y. Jin, B. Lee, and T. Hibino, *J. Jpn. Petrol. Inst.*, **53**, 12 (2010).
- O. Paschos, J. Kunze, U. Stimming, and F. A. Maglia, *J. Phys. Condens. Matter*, **23**, 234110 (2011).
- X. Wu, M. Mamlouk, and K. Scott, *Fuel Cells*, **11**, 620 (2011).
- H. Su, S. Pasupathi, B. Bladergroen, V. Linkov, and B. G. Pollet, *Int. J. Hydrogen Energy*, **38**, 11370 (2013).
- W. J. Lee, J. S. Lee, H. Y. Park, H. S. Park, S. Y. Lee, K. H. Song, and H. J. Kim, *Int. J. Hydrogen Energy*, **45**, 32825 (2020).
- S. Liu, K. Wippermann, and W. Lehnert, *Int. J. Hydrogen Energy*, **46**, 14687 (2021).
- H. Sumi, Y. Nakano, Y. Fujishiro, and T. Kasuga, *Int. J. Hydrogen Energy*, **38**, 15354 (2013).
- H. Sumi, *J. Ceram. Soc. Jpn.*, **125**, 829 (2017).
- I. Szczygiel and T. Znamierowska, *J. Therm. Anal. Calorim.*, **36**, 2195 (1990).
- J. Zhu, W. D. Cheng, and H. Zhang, *Acta Crystallographica E*, **64**, i74 (2008).
- T. V. Anfimova, "Metal phosphates as proton conducting materials for intermediate temperature fuel cell and electrolyser applications (PhD Thesis)." Technical University of Denmark (Denmark) (2014).
- T. Aulich, J. Thakare, J. Hurey, X. Wu, Z. Zhou, and O. Zholobko, (2021), US Patent No.
- M. Rzaigui, N. K. Ariguib, M. T. Averbuch-Pouchot, and A. Durif, *J. Solid State Chem.*, **52**, 61 (1984).
- M. T. Averbuch-Pouchot and A. Durif, *Topics in Phosphate Chemistry*. (World Scientific, Singapore) (1996).
- S. Phadke, J. C. Nino, and M. S. Islam, *J. Mater. Chem.*, **22**, 25388 (2012).
- T. S. Chung, *J. Macromol. Sci. C: Polym. Rev.*, **37**, 277 (1997).
- O. Zholobko, X. F. Wu, Z. Zhou, T. Aulich, J. Thakare, and J. Hurley, *J. Appl. Polym. Sci.*, **137**, 49639 (2020).
- ASTM D882-18 standard test method for tensile properties of thin plastic sheeting (ASTM International, West Conshohocken, PA) (2018).
- X. F. Wu and Y. A. Dzenis, *Int. J. Fracture*, **112**, L9 (2001).
- X. F. Wu and Y. A. Dzenis, *Compos. Struct.*, **70**, 100 (2005).
- X. F. Wu and O. Zholobko, *J. Compos. Sci.*, **4**, 173 (2020).
- M. Bukartyk, O. Zholobko, and X. F. Wu, *ACS Omega*, **7**, 5883 (2022).
- M. Rzaigui and N. K. Ariguib, *J. Solid State Chem.*, **56**, 122 (1985).
- J. Zhu, W. D. Cheng, and H. Zhang, *Acta Cryst. E*, **64**, i74 (2008).
- M. Rzaigui and N. K. Ariguib, *J. Solid State Chem.*, **52**, 61 (1984).
- H. Onoda, H. Nariai, H. Maki, and I. Motooka, *Phosphorus Res. Bull.*, **9**, 69 (1999).
- A. A. Hanna, S. M. Mousa, G. M. Elkomy, and M. A. Sherief, *Euro. J. Chem.*, **1**, 211 (2010).
- H. P. Weber, B. C. Tofield, and P. F. Liao, *Phys. Rev. B*, **11**, 1152 (1975).
- T. Kobayashi, T. Sawada, H. Ikeo, K. Muto, and J. Kai, *J. Phys. Soc. Jpn.*, **40**, 595 (1976).
- J. P. Budin, A. Milatos-Roufos, N. D. Chinh, and G. L. Roux, *J. Appl. Phys.*, **46**, 2867 (1975).
- Q. R. Cai, G. X. Lan, H. F. Wang, and G. Y. Hong, *J. Phys. Chem. Solids*, **51**, 279 (1990).